On the Electrostatic Equilibrium of Granular Flow in Pneumatic Conveying Systems

Jun Yao
Singapore-MIT Alliance, E4–04-10, 4, Engineering Drive 3, Singapore 117576

Yan Zhang
Dept. of Chemical and Biomolecular Engineering, National Univ. of Singapore, 4 Engineering Drive 4, Singapore 117576

Chi-Hwa Wang
Singapore-MIT Alliance, E4–04-10, 4, Engineering Drive 3, Singapore 117576; and Dept. of Chemical and Biomolecular Engineering, National Univ. of Singapore, 4 Engineering Drive 4, Singapore 117576

Yung C. Liang
Dept. of Electrical and Computer Engineering, National Univ. of Singapore, Kent Ridge Crescent, Singapore 119260

DOI 10.1002/aic.10991
Published online September 14, 2006 in Wiley InterScience (www.interscience.wiley.com).

An analytical methodology involving the concept of "electrostatic equilibrium" is developed for granular flow in pneumatic conveying systems. The methodology can be used for estimation of the electrostatic field distribution at various sections of the system and explanation of the mechanisms involved for various electrostatic phenomena observed. For all cases conducted in the conveying system, there was a "charging time" required for the system to reach the state of "electrostatic equilibrium." Experiments conducted at different sections of the system showed that the time required increased in the order: horizontal pipe, vertical pipe, and pipe bend. Through a physical analysis, it is deduced that electrostatic equilibrium is related to the granules' behavior and local flow characteristics. In general, a longer time duration taken to reach equilibrium corresponds to a process with more complicated granular flow patterns. In the electrostatic equilibrium state, the field distribution shows the highest electrostatic field strength near the pipe wall, and this field strength degrades from the pipe wall to the pipe center. At various pipe sections, the highest strength occurs at the bend, in accord with observations that electric sparking first occurs at that location within the entire pneumatic conveying system. In the vertical pipe, granular distribution was measured using electrical capacitance tomography (ECT), and granular velocities were cross-referenced with those using particle image velocimetry (PIV). The electrostatic force at low air flow rates is found to be the primary cause for granules sticking to the pipe wall and results in the formation of the half-ring or ring structure. The state of electrostatic equilibrium is physically influenced by several elements in conveying systems. In a cyclic conveying system, a new pipe (or low humidity or no antistatic agent) tends to expedite the process to reach electrostatic equilibrium and attain high magnitude of electrostatic current at the state. In a non-cyclic horizontal conveying system, a thin film (pipe) is found to prolong the process duration to reach equilibrium, while the case with charged film (pipe) takes shorter duration to do so. © 2006 American Institute of Chemical Engineers *AIChE J,* 52: 3775–3793, 2006

Keywords: electrostatics, equilibrium, granule, pneumatic conveying

Introduction

Flows of solid particulate systems have a natural tendency to acquire electrostatic charges through triboelectrification due to repeated collisions between particles with surfaces of a different material type.[1] This charging process should be responsible for many phenomena occurring in them, such as solid clustering,[2] ignition hazard,[3] and so on. Ciborowski and Wlodarski[4] measured the electrostatic potential in fluidized beds of polyvinyl acetate, polystyrol, and sand. They found that the electrode potential in a fluidized bed stabilized 20-30 min after the velocity and humidity of the fluidizing air became established.

Correspondence concerning this article should be addressed to C.-H. Wang at chewch@nus.edu.sg.

Yao et al.[5] characterized and quantified electrostatic charges associated with bubble motion in beds of fluidized polyethylene powder. They demonstrated that the addition of antistatic powders (1wt%) decreased both the standard deviation of the voltage signals and the net charge transfer rate within 1h in the polyethylene resin bed. Both of these results suggest that charge "equilibrium" may be obtained after several minutes to an hour in solid-handling systems. "Equilibrium" theory is important to estimate the maximum electrostatic charge carried by particles/pipe wall in particulate systems and helps to evaluate electrostatic energy reserved in the systems. However, it has not received proper attention in the literature and remains far from complete understanding. The present work aims to investigate the "electrostatic equilibrium" in pneumatic conveying systems and then use this concept to perform comprehensive evaluation for electrostatic energy and associated phenomena.

As a common phenomenon taking place in fluidized beds, electrostatics has attracted some research attention in recent years. Ciborowski and Wlodarski[4] used an electrode immersed in a fluidized bed from the top and found that the electrical potential was at its highest value when the electrode was located at the top of the settled bed before fluidization was initiated. In their experiments, excess electrostatic charge was dissipating near the top of the bed. Gajewski[6] set up a fluidized bed out of organic glass and then covered the inside with rings of copper sheet. Zones of electrostatic charge generation and dissipation were identified. He argued that the maximum charge dissipation occurs near the upper part of the fluidized bed and the collision of the particles against each other leads to "symmetric electrification," that is, some particles acquire positive charge and others negative charge. Jiang et al.[7] applied Gauss's law to spherical particles and calculated a theoretical maximum charge that a particle can carry. They concluded that the maximum theoretical electrostatic charge that can be built up on a particle surface is limited by the breakdown strength of the surrounding fluid. Zhang et al.[8] carried out a comprehensive study of the effects of electrostatic forces on cohesive particles in a dilute circulating fluidized bed system. Based on experimental data of instantaneous velocities of shale particles using a Laser Doppler Anemometer system, they found that the particles oscillate about the mean values in a chaotic manner. The velocity distribution could be approximated by the Maxwellian distribution function, and kinetic theory was a very promising approach to describe gas/particle flow systems. For free bubbling fluidized beds, Yao et al.[5] found that the amplitude of the electrostatic charge voltage signals increases with superficial gas velocity but decreases with humidity. More recently, Chen et al.[9] developed a technique to determine the charge distribution surrounding a single rising bubble in a two-dimensional fluidized bed. Their new technique was independent of net charge buildup in the bed, not influenced by charge transfer such as with collision probes, and allowed the reconstruction of the complete charge distribution around bubbles. In addition, Wolny and Opalinski[10] studied the mechanism of electric charge neutralization by the addition of fines to a fluidized bed. According to this mechanism, the fines change the contact conditions between particles of the bed, and transfer electric charge between particles, thus causing neutralization of the whole bed. For example, anti-static powder Larostat-519 was used in fluidized beds[5,8,11] to decrease electrostatics.

In recent years, the behavior of granular material under electrostatic effect has been investigated. As a physical phenomenon to study, many researchers have interest in the behavior of small particles ($\ll$1mm) in a known electric field, where particles used are conductive and the electric field is obtained from a pair of plates with a/d voltage. They found that granular cluster pattern differs with the voltage set[12-14] and is affected by humidity.[15] A similar phenomenon was observed[2] for larger particles (2.8mm) where three characteristic aggregation patterns (clusters, half-ring, and ring) were formed in a vertical pipe due to electrostatic effects in a pneumatic conveying system. Al-Adel et al.[16] investigated the effect of static electrification on gas-solid flows in vertical risers and captured qualitative features of riser flows: core-annular particle distribution, annular particle downflow at low riser gas velocities, and annular upflow at high gas velocities. Joseph and Klinzing[17] demonstrated that the choking of granular flow is caused by electrostatic effect in vertical pneumatic transport. On the other hand, electrostatic effects are dependent on a variety of factors such as the physical, chemical, and electrical characteristics of the material used and ambient conditions. Smeltzer et al.[18] performed tests in a pneumatic conveying system using glass beads and found that at constant loadings, small particles exhibit greater electrostatic effects over large particles. Matsusaka et al.[19] developed a formulation for the variation of granule charging caused by repeated impacts on a wall and employed the formulation to granule charging in a granular flow where each granule carried a different amount of charge. They then analyzed theoretically the granule charge distribution. Recently, Yao and Wang[20] developed a method to investigate the effect of granular size and shape on the electrostatics in pneumatic conveying systems and demonstrated that the proposed method is a useful tool for characterization of electrostatics in general systems where granules are made up of complex combinations of different sizes and geometries.

In the present study, the concept of "electrostatic equilibrium" is investigated for three typical sections (horizontal pipe, bend, and vertical pipe) in a pneumatic conveying system where induced currents were measured using electrometers. Based on the equilibrium state established, electrostatic field strength at these sections and electrostatic force acting on granules at the vertical pipe are respectively calculated, and the results are used to explain the associated phenomenon observed. In addition, "electrostatic equilibrium" is physically characterized by working elements in the conveying systems, such as pipe material, pipe lifespan, humidity, with/without antistatic powder, pipe thickness, and pipe charging status.

Methodology

Experimental design and setup

Two conveying systems used in this work include a cyclic system in which pipe lines consist of horizontal pipes, pipe bends, and vertical pipes, and another non-cyclic system in which pipe lines only consist of horizontal pipes. In the cyclic system, working pipes were made of polyvinyl chloride (PVC) material and electrostatic currents were measured at three sections, that is, horizontal pipe, pipe bend, and vertical pipe. At the vertical pipe, particle distribution and particle velocity were captured using ECT and PIV, respectively. Based on the cyclic system, several factors, such as pipe material [PVC, polyeth-

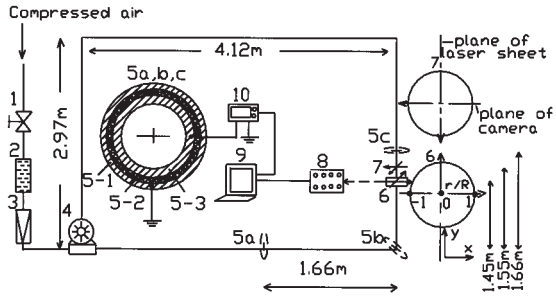

Figure 1. Experimental setup I.

(1) Air control valve; (2) air dryer (silica gel with indicator-blue); (3) rotameter; (4) rotary valve; (5a-c) induced current measurement: (5–1) aluminum foil sheet (0.07mm); (5–2) polymer film (0.04mm); (5–3) aluminum foil sheet (0.07mm); (6) ECT sensors location; (7) plane of PIV measurement; (8) ECT data acquisition module; (9) computer; (10) electrometer.

ylene (PE)], pipe status (new/old), ambient humidity (RH = 88%, 5%), and anti-static agent (Larostat-519 powder), were studied. In the non-cyclic system, working pipes were made of copper except at the test section where pipes were covered with a PE/polymethyl methacrylate (PPMA)/PVC film. Specific tests were carried out for this system to investigate the effect of film thickness (PE: 0.04, 0.12mm; PPMA: 0.12, 0.24mm), film pre-charging status (fresh/charged), and film material (PVC, PE) on the electrostatic characteristics for the conveying system.

The cyclic experimental setup with the full equipment list is shown in Figure 1. Solid granules are introduced into the rotary valve and entrained by air flowing from the compressor mains. The rotary valve (General Resource Corp., Hopkins, MN) has 8 pockets on the rotary and rotates at 30 rpm. The inner diameter of the pipe is 40 mm and the length of the vertical pipe section between two smooth 90° elbows (bend curvature: 2) is 2.97 m, while the horizontal section is 4.12 m in length. The transparent conveying pipe is made of PVC to allow visual observation and has a wall thickness of 5 mm. Induced current measurements (5 a-c) were mounted on three sections: one was at the horizontal pipe 1.66 m away from the downstream bend, one was at the bend, and the other was at the vertical pipe 1.66 m away from the bottom elbow. One set of 12-electrode ECT sensors (6) was mounted on the vertical pipe 1.45 m away from the bottom elbow. The plane of measurement for PIV was set at the vertical pipe 1.55 m from the bottom elbow. Transparent pipe fits the requirement of PIV for penetration of laser beam in the pipe. The entire configuration was held in position using metal castings and supported with various pipe segments joined by connectors and reinforced by silicone gel. Polypropylene granules (PP, diameter 2.8 mm, bulk density 1123 kg/m^3) with and without anti-static powder (Larostat-519 powder) were used throughout the experiments.

Air from the compressor mains (air pressure: 75 psi) flowed through the rotary feeder, driving granules to be fed into the conveying system. A valve (1) was used to adjust the air flow rate. The air flow rate was also controlled via a rotameter (3), which allowed a maximum flow rate of 2000 L/min. Based on a previous work,[2] three air flow rates were chosen: 1600, 1100, and 950 L/min, and the corresponding air superficial velocity inside the pipe was 21.20, 14.59, and 12.60 m/s. The air humidity was controlled by the dryer (silica gel with indicator-blue, labeled 2 in Figure 1) at a relative humidity, RH = 5%, and this was checked using a high performance digital thermo-hygrometer (RH411, OMEGA Technologics Ltd.) before and after each test. Ambient temperature was controlled at 28 ~ 30°C. For all cases conducted, the mass of granular material was 1100 g.

During the pneumatic conveying process, collisions between the solid granules and the pipe wall generate electrostatic charges. The current induced along the surface of the pipe wall as a result of these charges was measured as a function of time. This was done by wrapping an aluminum foil sheet tightly over the outer wall of the PVC pipe (5a-c). A coaxial line (connected to the high input end of an electrometer, Advantest R8252 Digital Electrometer) was connected to the outer surface of the aluminum foil sheet. A polymer film was then wrapped tightly over the aluminum foil sheet to separate this sheet from another aluminum foil sheet whose external surface was connected to the low input end of a coaxial cable. Subsequently, this external layer of aluminum foil sheet was connected to ground and then used as an extra electric shield. The induced current through the pipe wall was measured as a function of time through digital readings from the electrometer and stored in a computer at intervals of 0.5 s. The charge density of the particles was measured by a Faraday Cage (TR8031). The mass of granules collected in the cage was measured using an electronic balance to an accuracy of 10^{-4} g and the mass-to-charge ratio of the granules was then calculated.

Electrical capacitance tomography (ECT) measurement

ECT data were acquired using a data acquisition module (Process Tomography, Wilmslow, Cheshire, UK) connected to the ECT sensors; capacitance data were gathered under various operating conditions. The ECT was sampled at 40 Hz and the data were acquired for 30s for each experimental run.

As the local volume fraction of the solids divided by the volume fraction of particles at maximum packing, F_p (=0.77 for polypropylene particles), α_S (x,y,z,t) was obtained from post-processing of ECT data for each instant of time (t) using the simultaneous iterative reconstruction technique (SIRT) given by Su et al.[21] x and y denote the Cartesian coordinates in the cross-sectional plane (Figure 1) and were normalized using the pipe diameter as the characteristic length. The axial coordinate z denotes the location of the ECT electrodes. Henceforth, we will refer to α_S (loosely) as particle concentration, and the solids volume fraction is simply $\alpha_S \cdot F_p$. The time-averaged particle volume fraction values ($\bar{\alpha}_t$) were generated by averaging α_S (x,y,z,t) over a time period T (in this work, the 30 s of data acquired for each run):

$$\bar{\alpha}_t(x, y, z) = \frac{1}{T}\int_0^T \alpha_S(x, y, z, t)dt \qquad (1)$$

The instantaneous value of the cross-sectional average particle concentration $\bar{\alpha}_s(z, t)$ is defined as[22,23]:

$$\bar{\alpha}_s(z, t) = \frac{1}{A}\iint \alpha_S(x, y, z, t)dxdy \qquad (2)$$

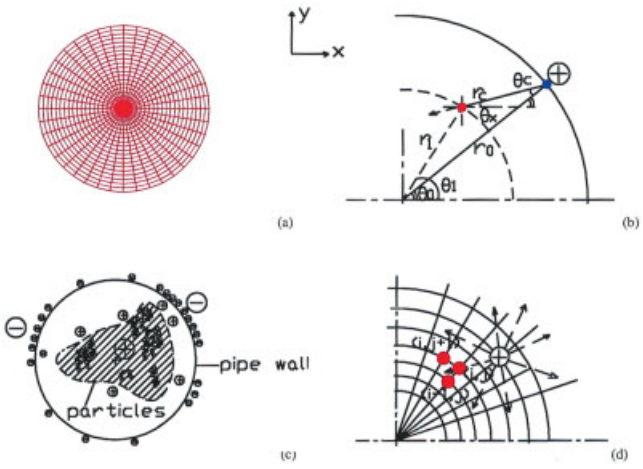

Figure 2. Electrostatic field calculation.

(a) Simulation grid (20 × 40); (b) the electrostatic field vector at one point (r_1, θ_1) due to a positive point charge (r_0, θ_0); (c) schematic of charges generated at the pipe wall and granules at the cross section of the pipeline in the pneumatic conveying system; (d) the electrostatic field vector at several points around a positive point charge (r_0, θ_0). [Color figure can be viewed in the online issue, which is available at www.interscience.wiley.com.]

and the time-average value of $\bar{\alpha}_s(z, t)$ is denoted by $<\alpha>(z)$:

$$\langle\alpha\rangle(z) = \frac{1}{T}\int_0^T \bar{\alpha}_s(z, t)dt \equiv \frac{1}{A}\iint \bar{\alpha}_t(x, y, z)dxdy \quad (3)$$

Particle Image Velocimetry (PIV) measurement

Measurements using a PowerView 2D PIV system from TSI Company (Shoreview, MN) were conducted at the vertical pipe region 1.55 m downstream from the bend. The laser light sheet generated by the Laser Pulse™ Solo Mini Dual Nd: YAG laser was introduced from the sidewall to lighten the granules at the center plane (Figure 1 (7)]. Images of the granules were captured by a PowerView™ 4M 2K×2K camera at the direction perpendicular to the lightsheet and sent to the computer for processing. The cross-correlation yields the distance traveled by the granules in a very small time interval ($dT = 100\ \mu s$) from the first snapshot to the second, and the velocity distribution of granules in the plane can be determined by dividing by the time interval. In this study, the variation of velocity in the axial direction of the vertical pipe was measured.

Electrostatic field

The electrostatic field strength by a point charge at the cross section of pipe (Figure 2a) can be expressed by the following equation[24]:

$$e = \frac{1}{4\pi\varepsilon_0}\cdot\frac{q}{r_c^2} \quad (4)$$

where ε_0 is the permittivity (in vacuum $8.85 \times 10^{-12}\ C^2/N{\cdot}m^2$), r_c is the distance from the point charge, and q is the point charge. It is clear that the electrostatic field strength reduces quadratically with the increasing distance r_c. Based on a simplified analysis shown in Appendix A, the contributions from other cross sections in the z-direction are much weaker than that from the local cross section. Henceforth, this work calculated the electrostatic field strength at the local section and neglected the contributions from other axial cross sections.

The charge point (r_0, q_0), object point (r_1, q_1), and field reference center [(0,0)] are shown in Figure 2b. The distance r_c between the charge point and object point can be calculated using the cosine rule:

$$r_c^2 = r_1^2 + r_0^2 - 2\cdot r_1\cdot r_0\cdot\cos(\theta_0 - \theta_1) \quad (5)$$

where r_1 and r_0 are the distances of the object point and charge point to the reference center, respectively. θ_1 and θ_0 are the radians of object and charge points respectively with reference to the center origin. The orientation of the electrostatic field vector at the object point (r_1, θ_1) can then be calculated by Eq. 6 using the sine rule in this triangle (Figure 2b):

$$\frac{r_c}{\sin|\theta_0 - \theta_1|} = \frac{r_1}{\sin\theta_c}$$

$$\theta_c = \arcsin\left(\frac{r_1\cdot\sin|\theta_0 - \theta_1|}{r_c}\right)$$

$$\theta_x = \theta_0 - \theta_c \quad (6)$$

where θ_c (Figure 2b) is the angle between the direction of the electrostatic field vector and that of the charge point to the field reference center, and θ_x is the angle between the direction of the electrostatic field vector and the x- axis. Henceforth, the electrostatic field vector in the x- and y- directions can be obtained:

$$e_x = e\cdot\cos\theta_x = \frac{1}{4\pi\varepsilon_0}\cdot\frac{q}{r_c^2}\cdot\cos\theta_x;$$

$$e_y = e\cdot\sin\theta_x = \frac{1}{4\pi\varepsilon_0}\cdot\frac{q}{r_c^2}\cdot\sin\theta_x \quad (7)$$

Based on previous triboelectrification experiments in the pneumatic conveying system using PP granules and PVC pipes,[2,25] it can be deduced that positive charges are generated on the PP granule surface while equal amounts of negative charges are accumulated on the PVC pipe wall (Figure 2c). In the pipe cross section with grid level 20 × 40 (Figure 2a), the electrostatic field vector (Figure 2d) at the point (i,j) from the point charge (l, k) can be calculated by the following:

$$e_{x(l,k,i,j)} = \frac{1}{4\pi\varepsilon_0}\cdot\frac{q_{(l,k)}}{r_{c(l,k,i,j)}^2}\cdot\cos\theta_{x(l,k,i,j)}$$

$$e_{y(l,k,i,j)} = \frac{1}{4\pi\varepsilon_0}\cdot\frac{q_{(l,k)}}{r_{c(l,k,i,j)}^2}\cdot\sin\theta_{x(l,k,i,j)} \quad (8)$$

where i, l are coordinates in the radial direction in the range $1\sim m$ ($m = 20$); and j, k are coordinates in the polar direction in the

Table 1. Three Characteristic Granular Flows in the Pneumatic Conveying System

Air Flow Rate (L/min)	Granule Weight (g)	Solid Flow Rate (g/s)	Granule Charge Density $Q_{\rho m}$ (e-09 C/g)	Granule Surface Charge Density σ (e-09 C/m^2)
1600	1100	40.67 ± 3.29	1.22	0.64
1100	1100	21.87 ± 0.98	2.05	1.07
950	1100	14.50 ± 0.47	2.36	1.24

range $1\sim n$ ($n = 40$). From all point charges in the cross section of the pneumatic conveying system, the total electrostatic field at the point (i, j) can be calculated as:

$$E_{x(i,j)} = \sum_{l=1}^{m}\sum_{k=1}^{n} e_{x(l,k,i,j)} = \sum_{l=1}^{m}\sum_{k=1}^{n} \frac{1}{4\pi\varepsilon_0}\cdot\frac{q_{(l,k)}}{r^2_{c(l,k,i,j)}}\cdot\cos\theta_{x(l,k,i,j)}$$

$$E_{y(i,j)} = \sum_{l=1}^{m}\sum_{k=1}^{n} e_{y(l,k,i,j)} = \sum_{l=1}^{m}\sum_{k=1}^{n} \frac{1}{4\pi\varepsilon_0}\cdot\frac{q_{(l,k)}}{r^2_{c(l,k,i,j)}}\cdot\sin\theta_{x(l,k,i,j)} \quad (9)$$

where l ranges from $1 \sim m$ except i and k ranges from $1 \sim n$ except j.

The magnitude of the electrostatic field vector at point (i, j) can be obtained as:

$$E_{(i,j)} = \sqrt{E^2_{x(i,j)} + E^2_{y(i,j)}} \quad (10)$$

Granule charge

In the experiments, the granule charge density was measured by a Faraday cage for three air flow rates as shown in Table 1. As the granule volume is known (under the assumption of sphere), the uniform surface charge distribution can be calculated by the following:

$$\sigma = \frac{\rho_p\cdot V_p\cdot Q_{\rho m}}{S_p} = 1/3\cdot r_p\cdot\rho_p\cdot Q_{\rho m} \quad (11)$$

where V_p is the granule volume, r_p is the granule radius, S_p is the granule surface area, σ is the granule surface charge density, ρ_p is the granule density, and $Q_{\rho m}$ is the granule charge density.

For the three air flow rates, granule surface charge density is calculated using Eq. 11 and shown in Table 1.

In this work, granule charge distribution is assumed to be uniform over the surface area occupied by the granular material. The total amount of charge carried by the granule is calculated by the product of granular surface charge density, area occupied by granular material, and the corresponding solid volume fraction (quantified by ECT measurements).

Drag force F_D[26]

$$\vec{F}_D = \frac{3}{4}\cdot\frac{\rho_g m_p}{\rho_p D_p} c_D\cdot(\vec{u}_g - \vec{u}_p)\cdot|\vec{u}_g - \vec{u}_p|$$

If the particle shape is considered as spherical, then the above equation can be simplified as:

$$\vec{F}_D = \frac{\pi\rho_g D_p^2}{8} c_D\cdot(\vec{u}_g - \vec{u}_p)\cdot|\vec{u}_g - \vec{u}_p| \quad (12)$$

where ρ_g is the gas density, m_p is the mass of the particle, D_p is the diameter of the particles, and $\vec{u}_g$, $\vec{u}_p$ are the translational velocity vectors of the gas and particle, respectively.

The drag coefficient, C_D, is defined as:

$$c_D = \frac{24}{\mathrm{Re}_p}\cdot(1 + 0.15\cdot\mathrm{Re}_p^{0.687}) = \frac{24}{\mathrm{Re}_p} f_D \quad \mathrm{Re}_p \le 1000 \quad (13)$$

$$C_D = 0.44 \quad \mathrm{Re}_p > 1000 \quad (14)$$

where $\mathrm{Re_p}$ can be obtained by:

$$\mathrm{Re}_p = \frac{\rho_g D_p|\vec{u}_g - \vec{u}_p|}{\mu_g} \quad (15)$$

Electrostatic force F_E[24]

In Figure 2, as the electrostatic field strength at point (i,j) is known, the electrostatic force acting on this charged point can be calculated:

$$F_{Ex(i,j)} = E_{x(i,j)}\cdot q_{(i,j)}$$

$$F_{Ey(i,j)} = E_{y(i,j)}\cdot q_{(i,j)} \quad (16)$$

where $F_{Ex(i,j)}$ and $F_{Ey(i,j)}$ are the electrostatic force in the x- and y- direction, respectively; $E_{x(i,j)}$ and $E_{y(i,j)}$ are the electrostatic field strength in the x- and y- direction, respectively (provided by Eq. 9); and $q_{(i,j)}$ is the charge at the point (i,j).

Therefore, at the point (i, j), the magnitude of the electrostatic force vector can be obtained:

$$F_{E(i,j)} = \sqrt{F^2_{Ex(i,j)} + F^2_{Ey(i,j)}} \quad (17)$$

Results and Discussion

Averaged current

In this work, induced current at three air flow rates was measured in the pneumatic conveying system. The induced current is predominately determined by three factors: (1) the charges on the pipe wall, (2) the charged granules passing through the detection segment without contacting the pipe wall, and (3) the charging effect of granules that are in direct contact with the pipe wall due to impacts or through sliding and rolling. In reality, the second factor is negligible in the charge generation either on the pipe wall or granules. This can be explained as follows. When a charged granule approaches the detection segment, a quantity of charge equal to that carried by the

granule is induced on the detection segment; when the granule departs from the segment, these induced charges are discharged. Thus, there is no net charge generated during the process. To eliminate this factor, a concept of averaged current is proposed:

$$\bar{I} = \frac{1}{T}\int_0^T I \cdot dt \tag{18}$$

where I is the induced current measured from the electrometer and T is the time period.

The polarity of the induced current generated in the conveying system (Figure 3a-c) was found to fluctuate over both negative and positive values, and the mechanism was explained in our previous work.[2] Here, the averaged current values according to Eq. 18 at the three pipe sections are shown in Figure 3d-i. It is seen that, for all cases, the averaged current does reach a constant negative value over a period of time. This result seems reasonable because negative charges were found to be generated at the pipe wall by granule (PP)-wall (PVC) collisions.[2,25] Davies[27] studied charge generation on dielectric surfaces and found that PVC has fairly higher work function than PP and, hence, prefers to receive electrons as a result of such collisions. The establishment of a steady averaged current indicates a state of "electrostatic equilibrium."

Electrostatic equilibrium

Figure 3g-i shows that for all cases studied, the averaged current did undergo a transient state before reaching the state of electrostatic equilibrium, and the time taken to reach such a steady state varies with air flow rate and the specific pipe section. To facilitate the study of such a "charging process," a ratio of instantaneous averaged current to the final steady state value is defined as follows:

$$DI_{(h)} = \frac{|\bar{I}_{(h)} - \bar{I}_0|}{\bar{I}_0} \tag{19}$$

where $\bar{I}_{(h)}$ is the averaged current at the h^{th} moment and $\bar{I}_0$ is the steady (equilibrium) state current. $DI_{(h)}$ is the ratio of the averaged current at the h^{th} moment to the steady state value. In this work, $\bar{I}_0$ is assumed to be equal to the value of $\bar{I}_{(h)}$ at the end of the experiment. Here, the electrostatic equilibrium is assumed to be reached when $DI_{(h)}$ is less than or about 0.1.

In addition, charges generated on the pipe wall over a period of time T can be calculated as:

$$Q = \int_0^T I \cdot dt \tag{20}$$

The various quantities obtained at equilibrium for all cases are summarized in Table 2. It shows that in the pneumatic conveying system, the higher the air flow rate, the shorter the charging process. Such a trend is observed for all three pipe sections (horizontal, vertical, and bend). Furthermore, regardless of the air flow rate used, the horizontal pipe section reached the equilibrium state within the shortest time duration. This was followed by the vertical pipe section, while the bend section took the longest time to reach equilibrium. Except for the bend section, charges generated at the pipe wall increase with decreasing air flow rate at the equilibrium state. For the bend section, the highest charge generation occurs at the highest air flow rate.

The dimensionless quantity DI is used to evaluate the equilibrium for all cases with very different current magnitudes. The electrostatic equilibrium is assumed to be reached when this ratio is less than or about 10%. A fixed ratio is used throughout to facilitate the comparisons of all cases with various conditions. It should be noted that the selection of this ratio (10%) is arbitrary, but the sensitivity of the electrostatic equilibrium result is further investigated to ensure that the qualitative nature of behavior reported is not sensitive to this particular selection. As the ratio is set smaller ($<$10%), the time scales taken for all cases to reach the electrostatic equilibriums are longer and the same conclusion is obtained.

Physical analysis of the electrostatic equilibrium

It is known that granule-wall collisions in a conveying system lead to charge generation both on the surface of the granules and the pipe wall.[1] Such processes can be seen as giving rise to the charging effect. On the other hand, if granules and pipe wall are initially charged, charges on the surface of granules can be partly neutralized by those charges pre-existing on the pipe wall during granule-wall collisions. This can be seen as a discharging process. At the start of the pneumatic conveying experiments, granules and pipe wall were fairly fresh and carrying few charges so that they were easily charged by granule-wall collisions. This gave rise to the charging process. After certain time duration, charges accumulated on granules and the pipe wall, and the discharging effect became more significant. As the charging/discharging process reached an equilibrium state, the amount of charges on granules and the pipe wall became steady, thus attaining the "electrostatic equilibrium" mentioned above. It is known that such an equilibrium state is actually a "dynamic equilibrium." In the conveying system, there may be many factors affecting the electrostatic equilibrium, such as air flow rate, pipe material, pipe usage age, humidity, anti-static agent, pipe thickness, pipe charging status, and so on. In the experiments, the electrostatic equilibrium was also found to be different at different pipe sections in the conveying system.

From the above analysis (Figure 3g-i), high air flow rate will shorten the period to reach the electrostatic equilibrium in the conveying system. It can be explained by the higher frequency of granule-wall collisions at high air flow rates, which leads to a higher efficiency for the process charging and discharging to reach the equilibrium state.

In the conveying system, granules encounter the largest amount of granule-wall collisions at the bend (90°), where their trajectories are rather complex. In former works,[28-30] it was found that most particle-bend impacts occur on the outer wall, while fewer collisions occur on the left- and right-wall and the least on the inner wall. Therefore, it is reasonable to believe that charge generation due to granule-wall collisions is non-uniform at the bend. This is why it takes the bend the longest duration to reach the electrostatic equilibrium in the conveying

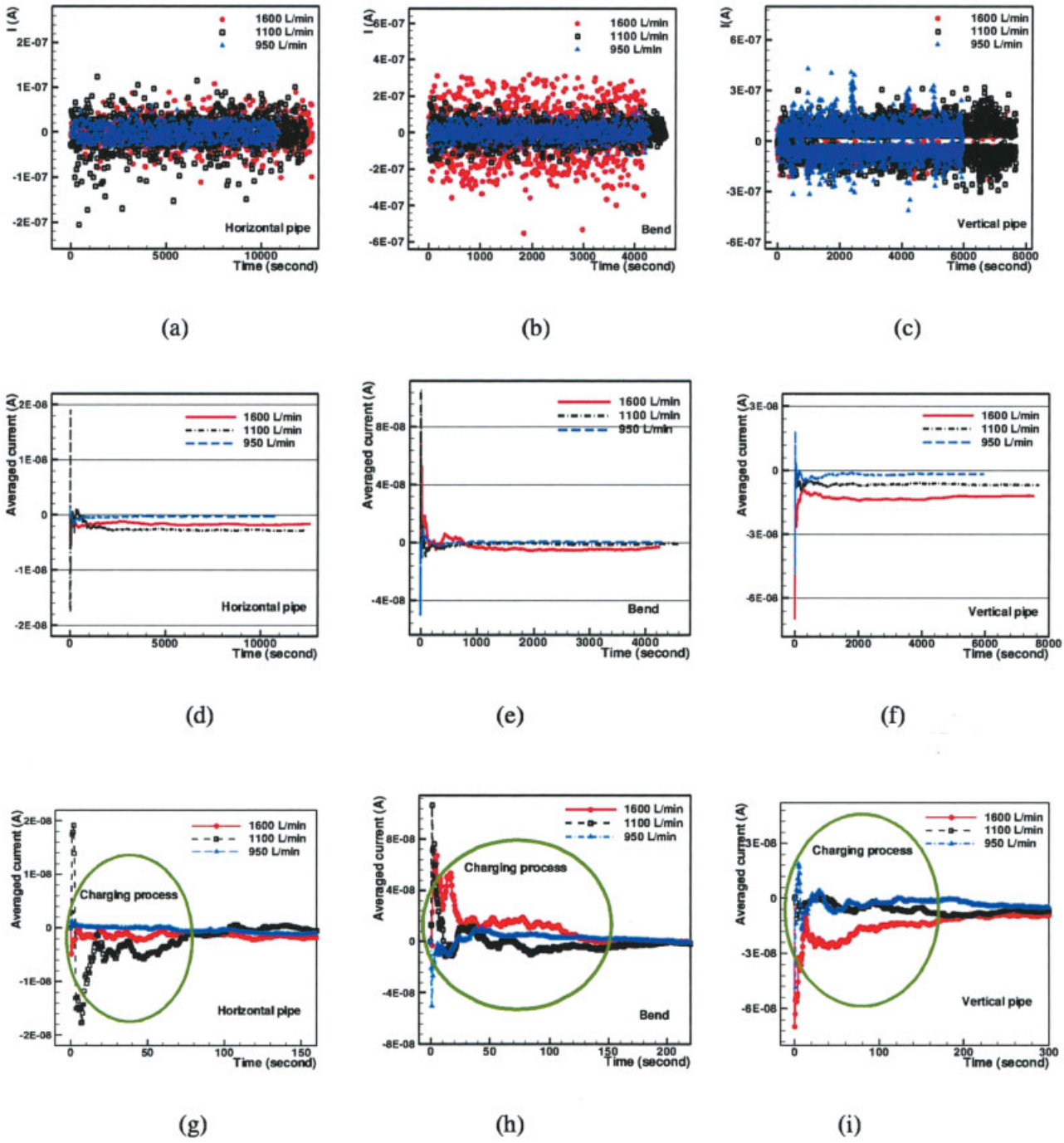

Figure 3. Electrostatics at the three pipe sections: horizontal, bend, vertical.

(a)-(c) Induced current; (d)-(f) averaged current; (g)-(i) charging process. [Color figure can be viewed in the online issue, which is available at www.interscience.wiley.com.]

system, as shown in Table 2. By the same reasoning, granular flow in the vertical pipe was found to be more complex than that at the horizontal pipe so that it takes more time for the former to reach the electrostatic equilibrium.[22,23,31,32] This statement can also be verified in Table 2. Henceforth, it can be deduced that the electrostatic equilibrium involving granule-wall collisions shows high relevancy to the granules' behavior and local flow characteristics (such as fluid turbulence): the more complex the granular flow, the longer to reach the electrostatic equilibrium state.

Electrostatic field

As the electrostatic equilibrium state is established, it is possible to evaluate the time-invariant electrostatic field strength in the pneumatic conveying system. According to Eqs.

Table 2. Electrostatic Equilibrium of Granular Flow in the Pneumatic Conveying System

Pipe Section	Air Flow Rate (L/min)	t_h (s)	$DI_{(h)}$	$\bar{I}_{(h)}$ (A)	Charge Q (C)	Pipe Wall Linear Charge Density λ (C/m)
Horizontal	1600	9.01	1.17E-01	−1.85E-09	−1.66E-08	−1.32E-07
Horizontal	1100	36.09	1.05E-01	−3.10E-09	−1.12E-07	−8.89E-07
Horizontal	950	663.88	4.99E-02	−3.07E-10	−2.04E-07	−1.62E-06
Vertical	1600	12.52	3.63E-02	−1.15E-08	−1.44E-07	−1.14E-06
Vertical	1100	60.31	9.33E-03	−6.82E-09	−4.11E-07	−3.27E-06
Vertical	950	1019.58	7.52E-02	−1.94E-09	−1.98E-06	−1.57e-05
Bend	1600	917.97	8.54E-02	−2.85E-09	−2.61E-06	−2.08E-05
Bend	1100	1132.57	7.34E-02	−6.59E-10	−7.46E-07	−5.93E-06
Bend	950	1756.13	9.99E-02	−2.86E-10	−5.02E-07	−3.99E-06

4-10, the electrostatic field strength from the charged wall was calculated for the three pipe sections: horizontal, bend, and vertical. The results are shown in Figure 4, where the charges are assumed to distribute evenly around the pipe wall. It is seen that, for all cases, the highest electrostatic field strength appears near the pipe wall and degrades from the pipe wall to the pipe center. In the conveying system, the highest strength occurs at the bend (Figure 4d-f), which is independent of air flow rate. For the horizontal pipe and vertical pipe, the electrostatic field strength increases with decreasing air flow rate. However, for the bend, the highest field strength occurs at the highest air flow rate. Basically, the electrostatic field strength in the conveying system is characterized by the amount of charges accumulated at the pipe wall at the electrostatic equilibrium. The larger the amount of charges accumulated, the higher the electrostatic field strength achieved.

In air, the electric breakdown potential is 3×10^6 V/m and the permittivity of air is 8.85×10^{-12} $C^2/N{\cdot}m^2$. The results achieved above (Figure 4) can be justified by the fact that electric sparks were frequently observed in the pneumatic conveying system and particularly occurred at the bend at high air flow rates. Spark was ever captured using the electrometer at the horizontal pipe around 30 min after running the conveying system. At the moment of sparking, the magnitude of induced current could reach as high as 6E-07 A. In comparison with horizontal pipe, it took a shorter period for sparks to occur at the vertical pipe and the bend as well as at a higher frequency. Working conditions were found to significantly affect spark occurrence. High solid flow rate, large particle, and low humidity would facilitate sparking in the conveying system.

Electrostatic effect on granular flows in the vertical pipe

In the pneumatic conveying system,[2] three different flow patterns corresponding to different air flow rates were observed at the vertical pipe, namely, the disperse flow, half-ring flow, and ring flow patterns. However, the working mechanism for the formation of these patterns has never been completely clarified. Here, attempts are made to characterize the electrostatics and compare the charge and particle distribution for the three types of flow using the concept of "electrostatic equilibrium" discussed above together with in-situ electrical capacitance tomography measurements.

ECT measurements of granule distribution

In this work, electrostatic charges are assumed to be uniformly distributed over the pipe wall. It can be shown that under such a special situation, the electrostatic effect on the accuracy of ECT measurement is negligible (see Appendix B). The transient measurement results (solids volume fraction = $Fp^*\bar{\alpha}_t$) from an ECT sensor at the vertical pipe for three air flow rates are shown in Figure 5. It shows that at a high air flow rate, 1600 L/min, granules tend to distribute in the core region ($0.3 < |r/R| < 1$), while at low air flow rates 1100, 950 L/min, granules have a fairly high congregation near the pipe wall ($|r/R| = 1$). Therefore, in the vertical section of the pneumatic conveying system, low air flow rates tend to increase granular distribution near the pipe wall, implying enhanced electrostatic force from the pipe wall.

Electrostatic field strength of charged granules

On the basis of granular distribution (Figure 5) and granule surface charge density (Table 1) described above, the electrostatic field strength of charged granules can be calculated using Eqs. 4-10, and the result is presented in Figure 6. According to the granular distribution at the high flow rate of 1600 L/min (Figure 6a), charged granules present high electrostatics near the core region. Conversely, at low flow rates of 1100, 950 L/min, the high electrostatic region is found to be near the pipe wall. Figure 6 also suggests that the electrostatic field strength of charged granules increases with decreasing air flow rate, which may be due to low air flow rate, high granule surface charge density, and high granular concentration.

The integrated electrostatic field strength accounting for both charged pipe wall and charged granules in the vertical pipe is presented in Figure 7. The results show that the electrostatic field strength degrades from the pipe wall to the pipe center. Such findings are consistent with the electrostatic field strength calculated from Eqs. 4-10 for charged pipe wall at the vertical pipe (Figure 4g-i). This is because the electrostatic field strength of the charged pipe wall (Figure 4) is three orders of magnitude higher than the charged granules (Figure 6). Therefore, it is reasonable to believe that in the vertical section of the pneumatic conveying system, the electrostatic strength of the charged pipe wall is dominant in the determination of the overall granular behavior.

Electrostatic force on granules

In the vertical pipe, electrostatic forces acting on granules at three typical air flow rates can be calculated according to Eqs. 16 and 17, and the results are plotted in Figure 8, where the

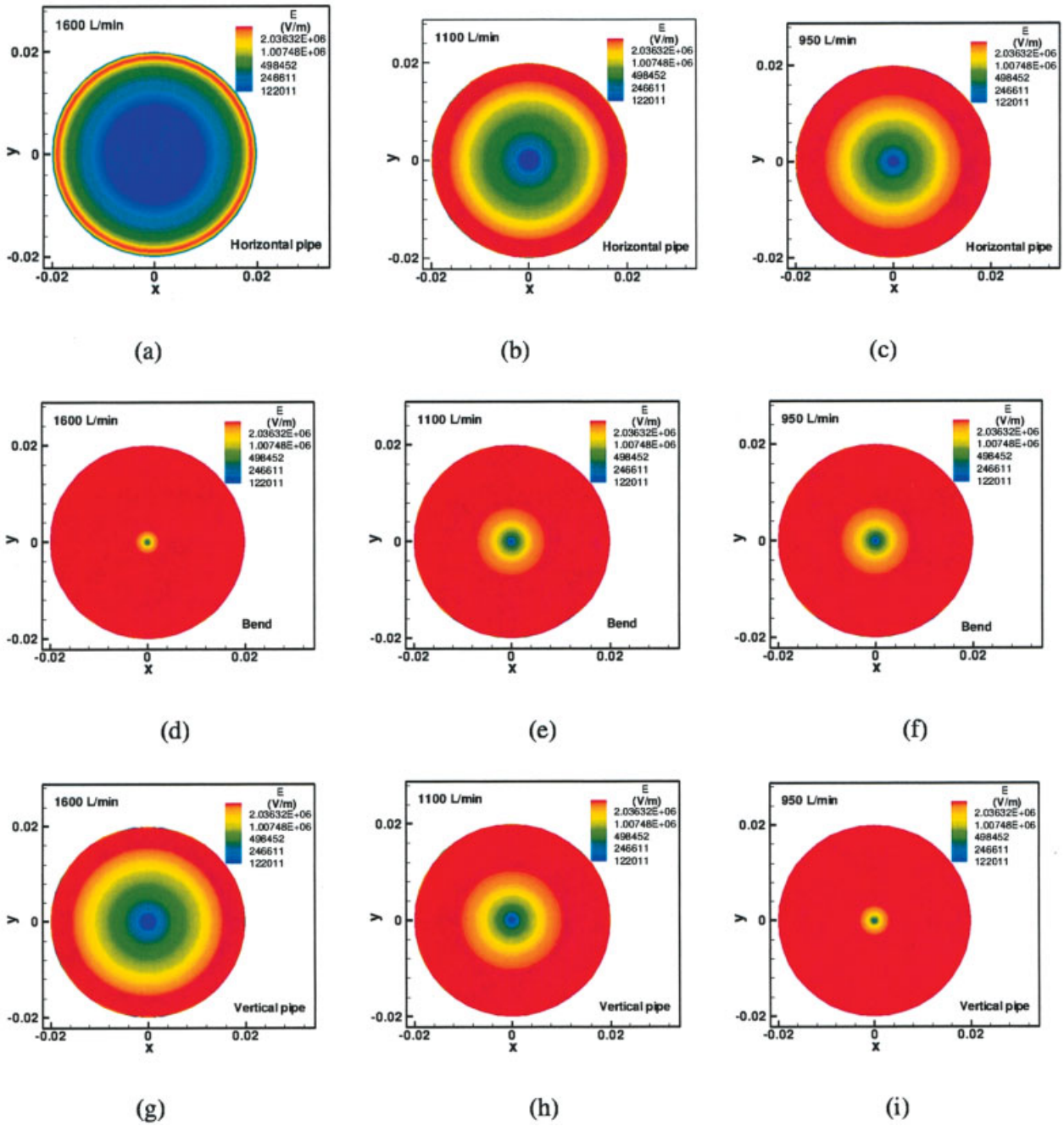

Figure 4. Electrostatic field strength of charged pipe wall at the equilibrium for the three flows (E = 1.22e5 ~ 1.22e7 V/m, 30 contour levels are given and scaled linearly between the minimum and maximum levels): 1600, 1100, 950 L/min.

(a)-(c) Horizontal; (d)-(f) bend; (g)-(i) vertical. [Color figure can be viewed in the online issue, which is available at www.interscience.wiley.com.]

granular concentration contour field is also presented. The electrostatic force is fairly high near the pipe wall and degrades from the pipe wall to the pipe center, and the results agree well with the distribution of the general electrostatic field strength in the vertical pipe (Figure 7). As air flow rate decreases, the electrostatic field strength of the charged pipe wall increases (Figure 4g-i), and this is accompanied by an increase in granule surface charge density (Table 1). Both factors mentioned above contribute to the enhancement of electrostatic forces (Figure 8) acting on granules and result in the high granular concentration near the pipe wall (Figure 5).

PIV measurement and dynamics analysis

For three typical flow patterns at the vertical pipe, granule velocities were measured using PIV. The averaged velocities of

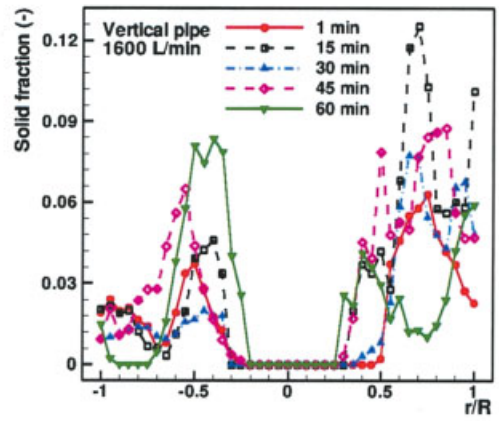

(a)

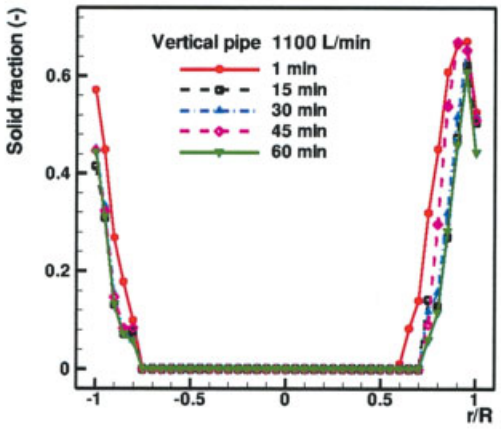

(b)

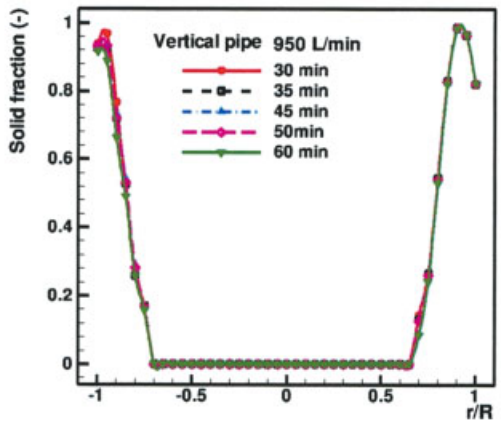

(c)

Figure 5. Radial distribution of the time averaged solids fraction (= Fp * $\overline{\alpha_i}$, data averaged for 30s, Fp = 0.77 for polypropylene particles) measured from an ECT sensor located at the vertical pipe (*z* = 1.45 m away from the bottom elbow) for three flow rates.

(a) 1600; (b)1100; (c) 950 L/min. r/R is depicted in Figure 1. [Color figure can be viewed in the online issue, which is available at www.interscience.wiley.com.]

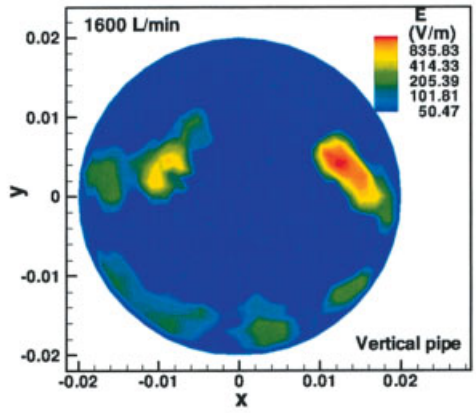

(a)

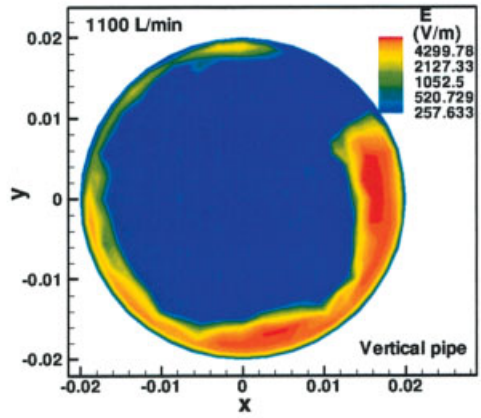

(b)

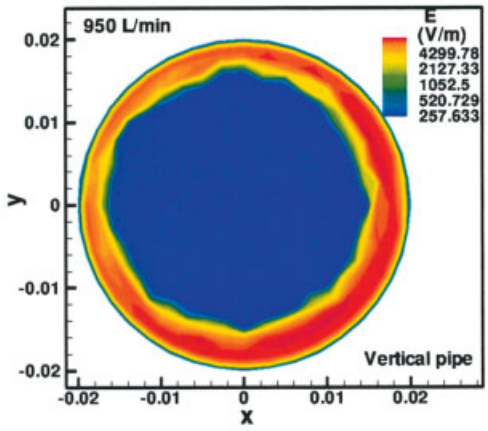

(c)

Figure 6. Electrostatic field strength of charged particles at the equilibrium at the vertical pipe for three flows.

(a) 1600 L/min (E = 50.47 ~ 1.51e3 V/m, 30 contour levels); (b) 1100 L/min (E = 2.65e2 ~ 7.95e3 V/m, 30 contour levels); (c) 950 L/min (E = 2.65e2 ~ 7.95e3 V/m, 30 contour levels). The *x*-*y* coordinate is depicted in Figure 1. [Color figure can be viewed in the online issue, which is available at www.interscience.wiley.com.]

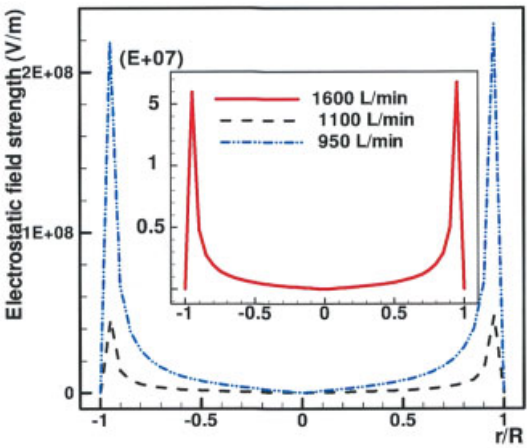

Figure 7. Radial distribution of general electrostatic field strength at the equilibrium at the vertical pipe.

r/R is depicted in Figure 1. [Color figure can be viewed in the online issue, which is available at www.interscience.wiley.com.]

granules in the core region ($r/R < 0.7$) and boundary region ($0.8 < r/R < 1$) are listed in Table 3. It is seen that granular velocities at the core region are obviously higher than those at the boundary region irrespective of air flow rates used in the conveying system. In addition, low air flow rate decreases granular velocity in the vertical pipe.

In the vertical section of the pneumatic conveying system, the main vertical forces acting on granules are gravity and fluid drag force. If the granule slides on the wall surface, frictional forces would act in the direction opposite to its motion. Based on the granule velocity measured using PIV, the fluid drag force acting on granules can be calculated using Eqs. 12-15. The electrostatic force acting on granules can be obtained using Eqs. 16 and 17. The frictional force is normal to the electrostatic force and its magnitude is equal to the electrostatic force multiplied by a dynamic friction parameter. As a result, all forces acting on granules in the vertical pipe are summarized in Table 3. It shows that in a disperse flow (air flow rate 1600 L/min), the air flow rate is sufficiently high for the magnitude of fluid drag forces to be much larger than that of gravitational forces in both the pipe core and boundary layer regions, so that granules do have fairly high upwards traveling speeds. Lower air flow rates give rise to the formation of half-ring and ring flows, and fluid drag forces within the wall boundary layer are reduced to about the same order of magnitude as that of gravitational forces, so that a dynamic equilibrium may be established between these two types of forces. Consequently, other types of forces such as the electrostatic force may then emerge as the dominant factor affecting granule behavior. In particular, the electrostatic force (F_E) represented by Eq. 17 above is seen to increase significantly (Table 3) due to the close proximity of the granules to the pipe wall at low air flow rates or high charge densities acquired by the pipe wall and granules. This demonstrates that electrostatics should be responsible for sticking granules to the pipe wall and forming the half-ring or ring structure at these flow rates.

Factors' effects on electrostatic equilibrium

Pneumatic Conveying System (Cyclic System). In this part, the experimental setup used was modified from the earlier configuration by removing the air dryer (labeled 2 in Figure 1)

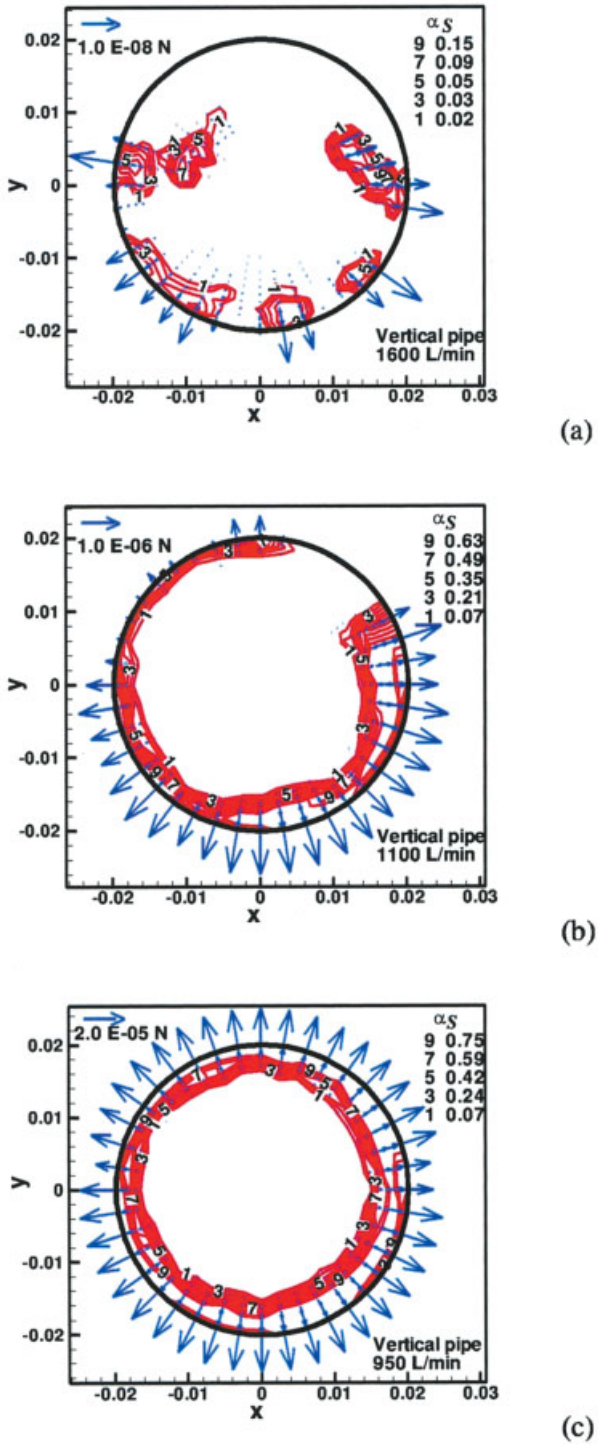

Figure 8. Electrostatic force acting on granules at the vertical pipe for three flows.

(a) 1600; (b)1100; (c) 950 L/min. The *x-y* coordinate is depicted in Figure 1. [Color figure can be viewed in the online issue, which is available at www.interscience.wiley.com.]

Table 3. Dynamic Analysis for a Granule in the Vertical Pipe of the Conveying System

	Air Flow Rate (L/min)	$\bar{v}_p$ (PIV) (m/s)	F_D (N)	F_E (N)	F_f (N)
Core region	1600	5.10	4.24E-04	4.68E-12 ~ 2.13E-09	—
	1100	0.30	3.33E-04	1.93E-10 ~ 3.82E-09	—
	950	0.15	2.53E-04	1.73E-08 ~ 1.03E-07	—
Boundary region	1600	3.60	2.12E-05	1.79E-09 ~ 2.23E-08	1.00E-09 ~ 1.25E-08
	1100	0.23	8.26E-08	9.39E-09 ~ 4.19E-06	5.26E-09 ~ 2.35E-06
	950	0.04	2.30E-09	6.42E-07 ~ 3.37E-05	3.60E-07 ~ 1.89E-05

Core region: $r/R < 0.7$; boundary region: $0.8 < r/R < 1$. Gravity of a granule: 1.27E-04 N. Friction acting on a granule touching the pipe wall: $F_f = F_E \cdot f$, where f is the friction parameter of PP-PVC, $f = 0.56$.

in the pneumatic conveying system (Figure 1). Air pressure at the inlet was controlled at 75 psi, and air flow rate and the corresponding air superficial velocity inside the pipe were chosen as 1600 L/min and 21.20 m/s, respectively. For all cases conducted, non-charged pipes were used and granule material was discharged for more than 24 h before any test. The mass of granular material was 1100 g.

Pipe Material. Figure 9a shows that the averaged currents at the electrostatic equilibrium stage are comparable for the pipe made of PVC and PE, although the time taken to reach the equilibrium is longer for PVC than PE. As a result, at the equilibrium state, more charges are found to be stored at the PVC pipe wall (Figure 9b). Thus, the material used for the pipes in a conveying system would be an important factor affecting the charge generation characteristics of the system.

Pipe Status (New/Old). In the pneumatic conveying system, the electrostatic charge generation mechanism of particles and pipe wall mainly depends on tribroelectrification.[2] The mechanical effect of particle-wall interactions gives rise to rough pipe wall and alters the electrostatic characteristics. For example, under strong mechanical impactions, the pipe wall may be in abrasion[29] and fine powders adhere to the pipe wall. In a previous work on conveying systems, deep gorges were found to be formed on the PE film (thickness: 0.04 mm) surface after 10 min usage.[2] In the present work, two pipes with different lifespan (old and new pipes) were introduced to characterize their respective performance. The old pipe was chosen after being used for more than 360 h, and the experimental results obtained for the new/old pipe are illustrated in Figure 10. It shows that in comparison with the new pipe, the old one needs more time to arrive at the electrostatic equilibrium (Figure 10a) and has a lower electrostatic current at that state, implying degraded electrostatics for the old pipe due to increasing surface roughness. Due to the much longer time taken to reach the equilibrium state, the total amount of charge accumulated on the surface of the pipe wall is larger for the old pipe (Figure 10b). As such, pipe status is another important factor affecting the charge generation characteristics of the pneumatic conveying system.

Humidity. The relative humidity (RH) of the ambient air is an important factor to be considered in any electrostatics experiment.[2,15,33,34] In the present work, both air from the ambient atmosphere (RH = 88%) and dry air (RH = 5%, by passing air through a silica gel column) were used. Experimental data were acquired at the vertical pipe and for all tests conducted for the same pipe (new/old). Figure 11 shows that high humidity prolonged the period to reach the equilibrium state and degraded the electrostatic current at that state. In other words, high RH of the conveying gas has a dampening effect on electrostatic charge generation. This claim is also supported by the fact that no half-ring or ring structure was visually observed when ambient air was used as the conveying medium, regardless of the flow rate used.

Anti-Static Agent (Larostat-519). A commercially available antistatic agent, Larostat-519 powder,[2,5,8,25] is found to be a suitable means to effectively control and reduce electrostatic effects in solid-handling processes. In comparison with cases where no such agent was used, the real current at electrostatic equilibrium in the presence of the Larostat-519 powder was

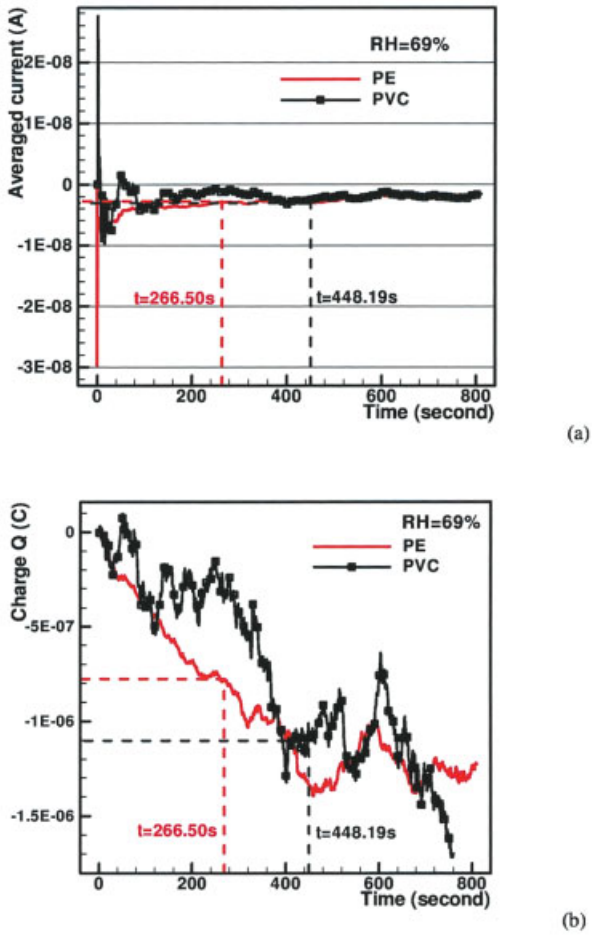

Figure 9. Pipe material effect on the electrostatic equilibrium at the horizontal pipe.

(a) Averaged current; (b) charges obtained by integration of induced currents. [Color figure can be viewed in the online issue, which is available at www.interscience.wiley.com.]

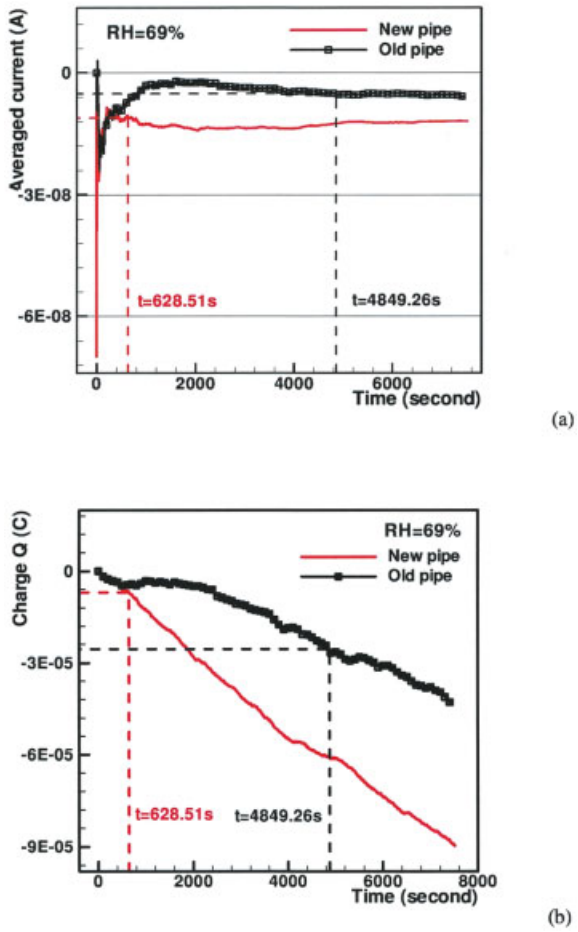

Figure 10. Pipe status (new/old) effect on the electrostatic equilibrium at the vertical pipe.

(a) Averaged current; (b) charges accumulation by the integration of induced currents. [Color figure can be viewed in the online issue, which is available at www.interscience.wiley.com.]

observed to be smaller by about three orders of magnitude (Figure 12a) and the time taken to arrive at the electrostatic equilibrium was observed to be longer. As a result, the amount of charges accumulated at the equilibrium state was smaller by about three orders of magnitude (Figure 12b). Therefore, Larostat-519 is confirmed to be of high anti-static effect in the pneumatic conveying system. The working mechanism was uncovered in a previous work.[2]

In the pneumatic conveying system, the total amount of charges accumulated at the pipe wall at the electrostatic equilibrium is proposed to be determined by two factors: the time duration taken to arrive at the equilibrium state and the electrostatic current at that state. From the above analyses, it is known that cases with strong electrostatic characteristics (new pipe, low humidity, without anti-static agent) tend to have higher magnitude of current at the electrostatic equilibrium state while a shorter time scale is needed to reach the state, and vice versa. This can be further explained by the fact that in cases with strong electrostatic characteristics, charges are more efficiently generated during the pneumatic conveying process and the ambient conditions facilitate higher charges transfer rates. However, the total amount of charges accumulated at the electrostatic equilibrium state is not necessarily higher for the case with strong electrostatics than in the weak electrostatics case because the duration of the charging process (to reach equilibrium) might have a stronger dependence on pipe material properties.

Horizontal Conveying System (Non-Cyclic System). The experimental setup shown in Figure 13 was used to investigate the electrostatic equilibrium of PP particles colliding with various films. The conveying pipes were made of copper except at the test section where pipes were covered with a PE/PMMA/PVC film. Figure 13 shows the detailed cross section of the test section following the design used by Matsusaka et al.[19] The various layers of materials consisted of PE (0.04, 0.12 mm)/PPMA (0.12, 0.24 mm)/PVC (0.12 mm), conductive adhesive (0.07 mm), and copper sheet (0.10 mm) as electrode, non-conductive adhesive (0.12 mm), and copper sheet (0.10 mm) as an electric shield. The copper electrode was connected to the Electrometer (R8252) and the electric shield was grounded. The whole conveying system was well grounded so that the particle charging conditions were kept constant during

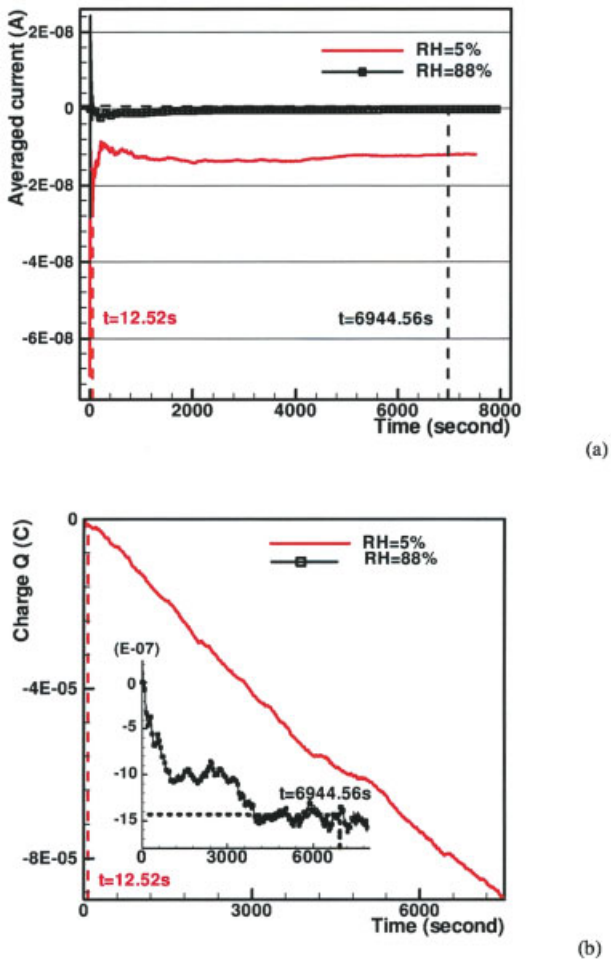

Figure 11. Humidity effect on the electrostatic equilibrium at the vertical pipe.

(a) Averaged current; (b) charges accumulation by the integration of induced currents. [Color figure can be viewed in the online issue, which is available at www.interscience.wiley.com.]

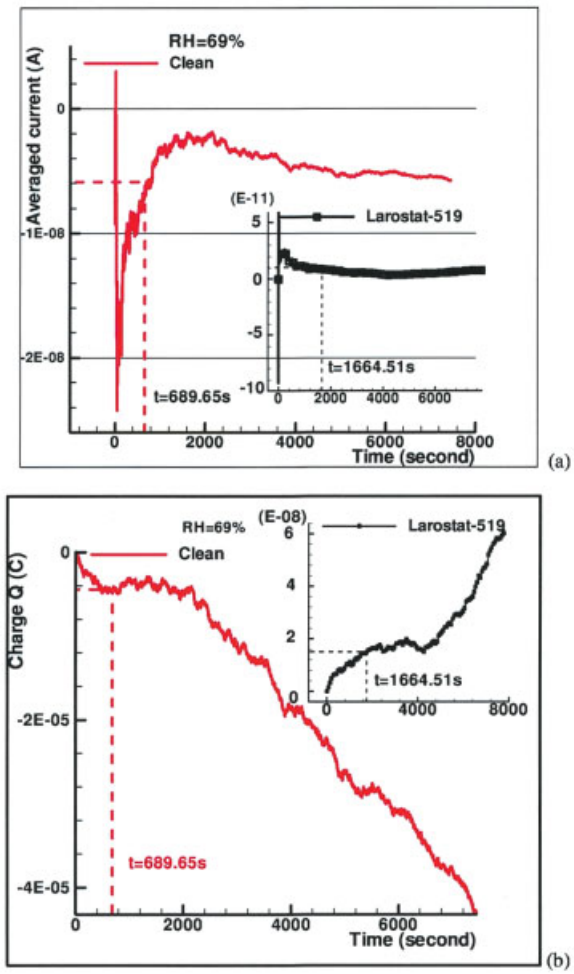

Figure 12. Anti-static agent (Larostat-519) effect on the electrostatic equilibrium at the vertical pipe.

(a) Averaged current; (b) charges accumulation by the integration of induced currents. [Color figure can be viewed in the online issue, which is available at www.interscience.wiley.com.]

their impacts with the metal wall. When the air pressure and flow rate were adjusted to 75 psi and 1600 L/min, respectively, particles passed through the horizontal pipe continuously at a rate of 44.4 ± 4.0 g/s. Electrostatic charge was generated at the test section, and the induced current was measured using the Electrometer (R8252) and stored in a computer at intervals of 0.1 s. All particles (1100 g) were collected in a metal container and grounded for discharging at the end of each experimental run.

Film Thickness. The effect of film thickness on the electrostatic equilibrium was investigated by comparing the behavior of the PE (PMMA) film with a thickness of 0.04 (0.12) mm and 0.12 (0.24) mm. Figure 14 shows that thick film facilitates faster establishment of the electrostatic equilibrium state and the electrostatic current at that state is fairly low. It indicates that, at electrostatic equilibrium, the amount of charge accumulated at the thick film is less than that accumulated at the thin film, regardless of the material used. Therefore, thin film may be more sensitive to electrostatic generation in comparison with thick film.

Pipe Pre-Charging Status. In real applications, residual electrostatic charges generated in conveying systems would be maintained for quite a long time after the systems are stopped. This might have some effect on the accuracy of electrostatic measurements of the conveying systems. In the present study, both initial case and charged case (initiated 70 min after the completion of the initial case) were conducted, and the results are presented in Figure 15. It shows that it takes more time for the initial case to reach electrostatic equilibrium than that for the charged case, while the electrostatic currents for both cases are of comparable level. Consequently, the amount of charges calculated for the equilibrium state is higher for the initial case in comparison with the charged case (Figure 15b). This is because the residual charges previously attained for the charged case decrease the requirement for extra charges to reach the equilibrium. In general, the total amount of charges stored at the film reaching electrostatic equilibrium is proposed to be at the same level (a material property) independent of charging status, either initial film or charged film.

Film Material. Following the work conducted in the pneumatic conveying system mentioned above, various film materials (PE, PVC) were tested in the horizontal conveying system and the results are presented in Figure 16. It shows that, in comparison with PE (thickness 0.12 mm), PVC (thickness: 0.12 mm) needed more time to reach electrostatic equilibrium where both materials had a similar level of averaged current. As such, more charges are suggested to be stored at PVC film at the equilibrium state (Figure 16b). This finding agrees with a previous statement achieved in the continuous pneumatic conveying system.

Conclusions

The conclusions derived from the present work can be briefly summarized as follows.

First, we propose a novel electrostatic characterization method based on the measurement of induced current from the pipe wall to examine the "charging process" and "electrostatic equilibrium state" for pneumatic conveying systems. High air flow rates actually shorten the charging progress. At various pipe sections, the sequence of reaching the equilibrium state from fast to slow is given by: horizontal, vertical, and bend. From a physical analysis, it is deduced that electrostatic equi-

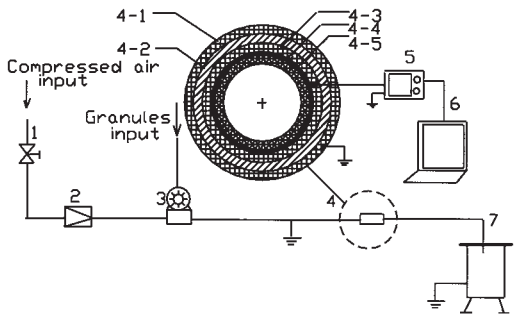

Figure 13. Experimental setup II.

(1) Air control valve; (2) rotameter; (3) rotary valve; (4) test segment: (4–1) copper electric shield (0.10mm); (4–2) nonconductive adhesive (0.12mm); (4–3) copper electrode (0.10mm); (4–4) conductive adhesive (0.07mm); (4–5) film tested; (5) electrometer; (6) computer; (7) metal container.

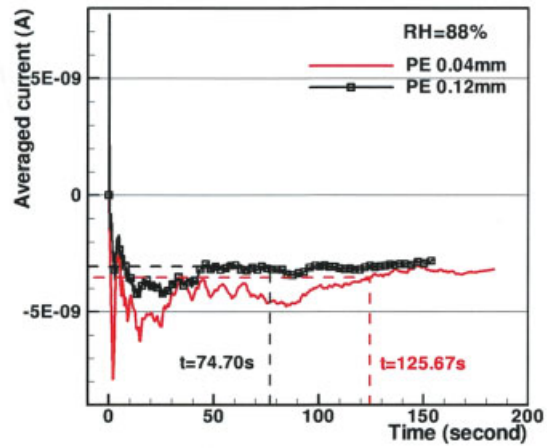

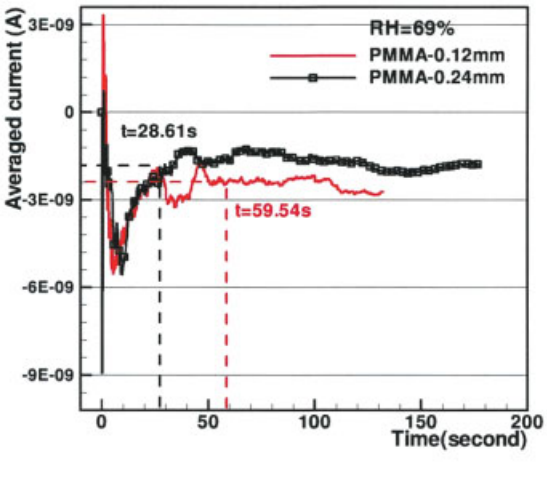

Figure 14. Film thickness effect on the electrostatic equilibrium (averaged current).

(a) PE; (b) PMMA. [Color figure can be viewed in the online issue, which is available at www.interscience.wiley.com.]

librium involving granule-wall collisions has strong dependence on the granules' behavior and local flow characteristics. In general, the time scale to reach electrostatic equilibrium increases with the complexity of the granular flow pattern.

Second, in the pneumatic conveying system, electrostatic energy analysis is carried out separately for the pipe wall and granules. For the charged pipe wall, the highest electrostatic field strength appears near the pipe wall and degrades from the pipe wall to the pipe center. At various pipe sections, the highest field strength does occur at the bend. For the horizontal pipe and vertical pipe, the electrostatic field strength increases with decreasing air flow rate. However, for the bend, the highest electrostatic field strength occurs at the highest air flow rate. Basically, the electrostatic field strength of the charged pipe wall is demonstrated by the amount of charge accumulated at the electrostatic equilibrium state. The larger the amount of charges accumulated, the higher the electrostatic field strength achieved. For charged granules, the electrostatic energy increases with increasing solid concentration.

Third, a dynamic analysis is carried out for charged granules in the vertical section of the pneumatic conveying system. It is found that the electrostatic force acting on granules is fairly high near the pipe wall and degrades from the pipe wall to the pipe center. Furthermore, the electrostatic force is found to increase with decreasing air flow rate and is responsible for causing granules to stick to the pipe wall and forming the half-ring or ring structure at low flow rates. In this work, the electrostatic energy in the vertical pipe is found to be mostly from the charges at the pipe wall.

Also, electrostatic equilibrium is physically characterized by working elements in the conveying systems, such as pipe material, pipe lifespan, humidity, anti-static agent, film (pipe) thickness, and film (pipe) charging status. In the pneumatic conveying system, high humidity is found to prolong the period to reach the electrostatic equilibrium state and lower the electrostatic current at that state. Larostat-519 is demonstrated to be of high anti-static effect due to around three orders of magnitude of charge reduction at the equilibrium state. Pipe material and pipe lifespan are also found to be important factors affecting the electrostatic equilibrium of the system. In the horizontal conveying system, thin film (pipe) is suggested to prolong the period to reach the equilibrium state and

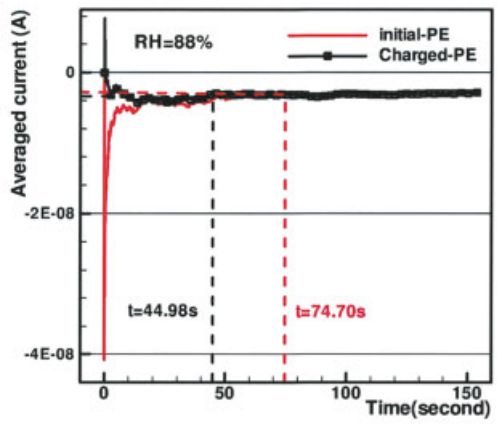

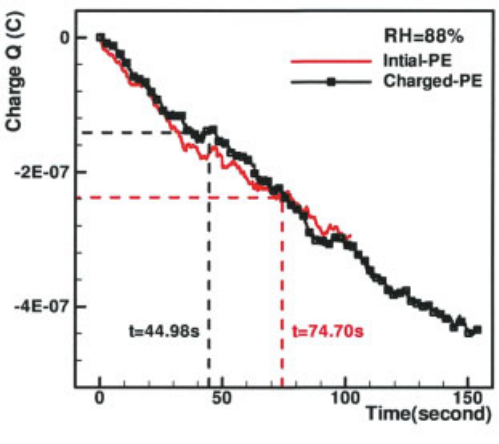

Figure 15. Charging status effect on the electrostatic equilibrium (PE thickness: 0.12mm).

(a) Averaged current; (b) charges accumulation by the integration of induced currents. The charged case was conducted 70 min after the initial case. [Color figure can be viewed in the online issue, which is available at www.interscience.wiley.com.]

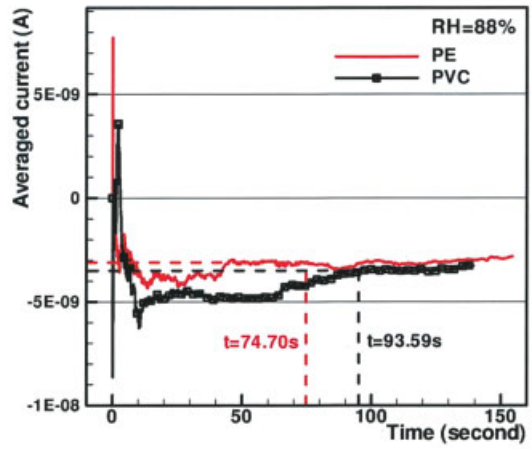

(a)

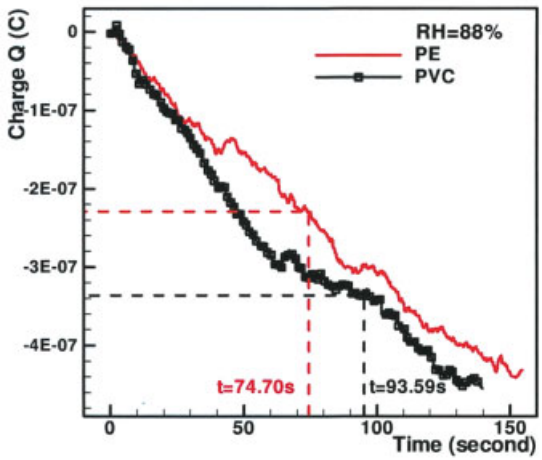

(b)

Figure 16. Film material effect on the electrostatic equilibrium (PE, PVC thickness: 0.12 mm).

(a) Averaged current; (b) charges accumulation by the integration of induced currents. [Color figure can be viewed in the online issue, which is available at www.interscience.wiley.com.]

increase the electrostatic current. Charged film (pipe) is found to shorten the period to reach the equilibrium state, while the electrostatic current at the state remains unchanged with that of original film (pipe).

Acknowledgments

This project was supported by the National University of Singapore and Singapore-MIT Alliance under grant numbers R279–000-208–305 and MEBCS project-003, respectively. We also extend our sincere thanks to Eldin Wee Chuan Lim for his assistance in the preparation of this manuscript.

Notation

A = area of pipe cross section, m^2
C_D = drag coefficient, dimensionless
D_p = particle diameter, m
DI = the ratio of the averaged current to the equilibrium value, dimensionless
e = electrostatic field strength of a point charge, N/C
E = integrated electrostatic field strength, N/C
e_x = electrostatic field strength in the *x*- direction, N/C
E_x = summation of electrostatic field strength in the *x*- direction, N/C
e_y = electrostatic field strength in the *y*- direction, N/C
E_y = summation of electrostatic field strength in the *y*- direction, N/C
f = friction parameter, dimensionless
F_D = drag force, N
F_E = electrostatic force, N
F_{Ex} = electrostatic force in the *x*- direction, N
F_{Ey} = electrostatic force in the *y*- direction, N
F_f = friction, N
F_p = volume fraction of particles at maximum packing, dimensionless
I = induced current, A
$\bar{I}$ = averaged current, A
m_p = mass of particle, g
q = point charge, C
Q = total charge, C
Q_{pm} = granule charge density, C/g
r = radial distance from the pipe axis, m
R = pipe radius, m
r_1 = distance between the object point and the reference center point, (0,0) m
r_0 = distance between the charge point and the reference center point, (0,0) m
r_c = distance between the point charge and object point, m
r_p = granule radius, m
Re_p = particle Reynolds number, dimensionless
S_p = surface area of granule, m^2
T = time period, s
u = translational velocity vector, m/s
V_p = volume of granule, m^3
$\bar{v}_p$ = averaged velocity of particles measured using PIV, m/s

Greek letters

ε_0 = permittivity constant, $C^2/N{\cdot}m^2$
θ_0 = radian of object point, dimensionless
θ_1 = radian of charge point, dimensionless
θ_c = angle between the direction of the electrostatic field vector and that of the charge point to the reference center point (0,0), dimensionless
θ_x = angle between the direction of the electrostatic field vector and the *x*- axis, dimensionless
σ = granule surface charge density, C/m^2
ρ = density, kg/m^3
μ = viscosity, kg m^{-1} s^{-1}
λ = pipe wall linear charge density, C/m
α_S = particle volume fraction, dimensionless
$\bar{\alpha}_s$ = cross-sectional average particle concentration, dimensionless
$\bar{\alpha}_t$ = time-averaged particle volume fraction value, dimensionless

Subscripts

g = fluid phase
h = h^{th} moment
i = i^{th} point in the radial direction (depicted in Figure 2)
j = j^{th} point in the polar direction (depicted in Figure 2)
l = l^{th} point in the radial direction (depicted in Figure 2)
k = k^{th} point in the polar direction (depicted in Figure 2)
p = granule

Literature Cited

1. Masuda H, Komatsu T, Iinoya K. The static electrification of particles in gas-solid pipe flow. *AIChE J.* 1976;22:558-564.
2. Yao J, Zhang Y, Wang CH, Matsusaka S, Masuda H. Electrostatics of the granular flow in a pneumatic conveying system. *Ind Eng Chem Res.* 2004;43:7181-7199.
3. Glor M. Ignition hazard due to static electricity in particulate processes. *Powder Technol.* 2003;135-136:223-233.
4. Ciborowski J, Wlodarski A. On electrostatic effects in fluidized beds. *Chem Eng Sci.* 1962;17:23-32.
5. Yao L, Bi HT, Park AH. Characterization of electrostatic charges in freely bubbling fluidized beds with dielectric particles. *J Electrostat.* 2002;56:183-197.

6. Gajewski A. Investigation of the electrification of polypropylene particles during the fluidization process. *J Electrostat.* 1985;17:289-298.
7. Jiang PJ, Bi HT, Liang SC, Fan LS. Hydrodynamic behavior of circulating fluidized bed with polymeric particles. *AIChE J.* 1994;40: 193-206.
8. Zhang YF, Yang Y, Arastoopour H. Electrostatic effect on the flow behavior of a dilute gas/cohesive particle flow system. *AIChE J.* 1996;42:1590-1599.
9. Chen AH, Bi HT, Grace JR, Willigen FK, Ommen JR. Measurement of charge distribution around a rising bubble in a 2-D fluidized bed. *AIChE J.* 2006;52:174-184.
10. Wolny A, Opalinski I. Electric charge neutralization by addition of fines to a fluidized bed composed of coarse dielectric P-articles. *J Electrostat.* 1983;14:279-289.
11. Chang H, Louge M. Fluid dynamic similarity of circulating fluidized beds. *Powder Technol.* 1992;70:259-270.
12. Yeh SR, Seul M, Shralman BI. Assembly of ordered colloidal aggregates by electric-field-induced fluid flow. *Nature (London).* 1997;386: 57-59.
13. Sapozhnikov MV, Tolmachev YV, Aranson IS, Kwok WK. Dynamic self-assembly and patterns in electrostatically driven granular media. *Phys Rev Lett.* 2003;90:114301.
14. Aranson IS, Blair D, Kalatsky VA, Crabtree GW, Kwok WK, Vinokur VM, Welp U. Electrostatically driven granular media: phase transitions and coarsening. *Phys Rev Lett.* 2000;84:3306.
15. Howell DW, Aronson IS, Crabtree GW. Dynamics of electrostatically driven granular media: effects of humidity. *Phys Rev E.* 2001;63: 050301.
16. Al-Adel MF, Saville DA, Sundaresan S. The effect of static electrification on gas-solid flows in vertical risers. *Ind Eng Chem Res.* 2002; 41:6224.
17. Joseph S, Klinzing G. E. Vertical gas-solid transition flow with electrostatics. *Powder Techno*l. 1983;36:79-87.
18. Smeltzer EE, Weaver ML, Klinzing GE. Individual electrostatic particle interaction in pneumatic transport. *Powder Technol.* 1982;33:31-42.
19. Matsusaka S, Nishida T, Gotoh Y, Masuda H. Electrification of fine particles by impact on a polymer film target. *Adv Powder Technol.* 2003;14:127-138.
20. Yao J, Wang CH. Granular size and shape effect on electrostatics in pneumatic conveying systems. *Chem Eng Sci.* 2006;61:3858-3874.
21. Su BL, Zhang YH, Peng LH, Yao DY, Zhang BF. The use of simultaneous iterative reconstruction technique for electrical capacitance tomography. *Chem Eng J.* 2000;77:37-41.
22. Rao MS, Zhu KW, Wang CH, Sundaresan S. Electrical capacitance tomography measurements on the pneumatic conveying of solids. *Ind Eng Chem Res.* 2001;40:4216-4226.
23. Zhu KW, Rao SM, Wang CH, Sundaresan S. Electrical capacitance tomography measurements on vertical and inclined pneumatic conveying of granular solids. *Chem Eng Sci.* 2003;58:4225-4245.
24. Halliday D, Resnick R, Walker J. *Fundamentals of Physics Extended*, 5th ed. New York: Wiley; 1997:558.
25. Zhu KW, Rao MS, Huang QH, Wang CH, Matsusaka S, Masuda H. On the electrostatics of pneumatic conveying of granular materials using electrical capacitance tomography. *Chem Eng Sci.* 2004;59: 3201-3213.
26. Sommerfeld M. Analysis of collision effects for turbulent gas-particle flow in a horizontal channel: Part I. Particle transport. *Int J Multiphase Flow.* 2003;29:675-699.
27. Davies DK. Charge generation on dielectric surfaces. *J Phys D: Appl Phys.* 1969;2:1533-1537.
28. Fan JR, Yao J, Cen KF. Antierosion in a 90° bend by particle impaction. *AIChE J.* 2002;48:1401-1412.
29. Lee LY, Quek TY, Deng RS, Ray MB, Wang CH. Pneumatic transport of granular materials through a 90° bend. *Chem Eng Sci.* 2004;59: 4637-4651.
30. Yao J, Zhang BZ, Fan JR. An experimental investigation of a new method for protecting bends from erosion in gas-particle flows. *Wear.* 2000;240:215-222.
31. Zhu KW, Wong CK, Rao SM, Wang CH. Pneumatic conveying of granular solids in horizontal and inclined pipes. *AIChE J.* 2004;50: 1729-1745.
32. Lim EWC, Wang CH, Yu AB. Discrete element simulation for pneumatic conveying of granular material. *AIChE J.* 2006;52:496-509.
33. Nieh S, Nguyen T. Effects of humidity, conveying velocity, and particle size on electrostatic charges of glass beads in a gaseous suspension flow. *J Electrostat.* 1988;21:99-114.
34. Guardiola J, Rojo V, Ramos G. Influence of particle size, fluidization velocity and relative humidity on fluidized bed electrostatics. *J Electrostat.* 1996;37:1-20.

Appendix A: Two-Dimensional Approximation of Electrostatic Field Strength

We attempt to analyze the contributions of electrostatic field strength from other cross sections in the z-direction with reference to the schematic diagrams shown in Figures A1 and A2.

The electrostatic field strength caused by a point charge at a fixed cross section of pipe (illustrated in Figure A1) can be expressed by the following:

$$e = \frac{1}{4\pi\varepsilon_0} \cdot \frac{q}{r_c^2} \tag{A1}$$

where ε_0 is the permittivity (in vacuum 8.85×10^{-12} $C^2/N{\cdot}m^2$), r_c is the distance from the point charge, and q is the point charge.

The electrostatic field strength reduces greatly with increasing charge-point separation (inversely proportional to the square of charge-point distance). Here, three charge points A (i_0, j_0, $k + 1$), B (i_0, j_0, k), and C (i_0, j_0, $k - 1$) are assumed to locate at the wall near to the point P (i, j, k) (see Figure A1). If all three cross sections in the z-direction are considered, the electrostatic field strength at the point (i, j, k) can be calculated as:

$$E_{(i,j,k)} = E_{Ax} + E_{Bx} + E_{Cx} = E_A \cdot \cos\theta + E_B + E_C \cdot \cos\theta \tag{A2}$$

where the electrostatic field strengths E_A, E_B, and E_C can be calculated by Eq. A-1.

Based on the following simplified analysis, it is known that the contributions from other cross sections in the z-direction (E_{Ax} and E_{Cx}) are much weaker than that from the local cross section (E_{Bx}) if the axial separation (h) is greater than 2.5 l_B.

$$E_{Ax} = E_A \cdot \cos\theta = \frac{1}{4\pi\varepsilon_0} \cdot \frac{q}{l_A^2} \cdot \frac{l_B}{l_A} = \frac{1}{4\pi\varepsilon_0} \cdot \frac{q \cdot l_B}{l_A^3} \tag{A3}$$

$$E_B = E_{Bx} = \frac{1}{4\pi\varepsilon_0} \cdot \frac{q}{l_B^2} \tag{A4}$$

$$\frac{E_{Ax}}{E_{Bx}} = \frac{\frac{l_B}{l_A^3}}{\frac{1}{l_B^2}} = \frac{l_B^3}{l_A^3} = \left(\frac{l_B}{\sqrt{l_B^2 + h^2}}\right)^3 \tag{A5}$$

$$\text{if } h > 2l_B, \frac{E_{Ax}}{E_{Bx}} < 9\%$$

$$h > 2.5l_B, \frac{E_{Ax}}{E_{Bx}} < 5\% \tag{A6}$$

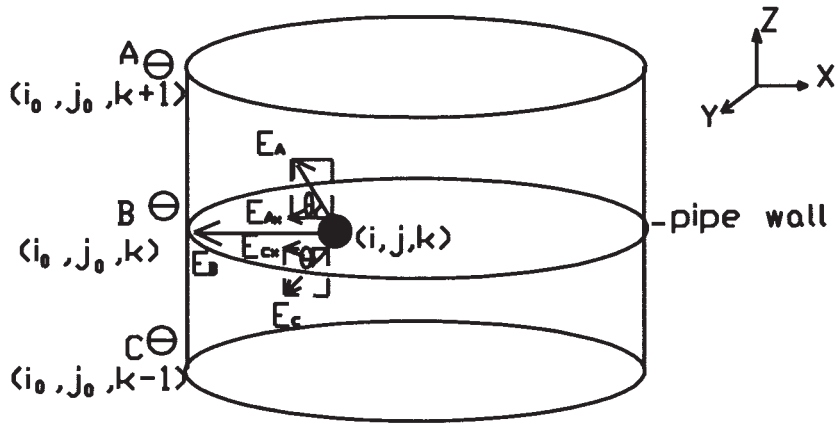

Figure A1. Contributions of electrostatic field strength from different cross sections in the *z*-direction.

The electrostatic field strength is higher for the region near the pipe wall ($l_B/R \leq 0.1$, see Figure 7) where the electrostatic forces acting on particles may have significant effect on their behavior. Therefore, for the case $h > 5$mm, ($l_B = 0.1R$, R = 20mm, $h > 2.51_B$), the contributions from other axial cross sections (EA_x and EC_x) are much weaker (<5%) than the one from charged particles at the same local cross section (E_{Bx}). It is understandable that the problem will be fully resolved if the contribution from other cross sections in the z-direction is considered for a more accurate solution.

Appendix B: Principle of Capacitance Measurements

For a 12-sensor ECT system, a total of 66 ($12 \times (12 - 1)/2$) capacitance [$\vec{C}$ (66,1)] measurements can be obtained for each cycle of measurements. These capacitances are determined by the solids distribution over the cross-section of the conveying pipe, which is divided into 32×32 "pixels."

In a charge/discharge cycle, for instance, between electrode 1 and electrode 2, switch S_1 is first closed to connect to a known voltage V (Figure B1) to charge the system capacitance C_{s12}. Once the charging process is completed, S_1 is opened and S_2 is closed to discharge the stored energy from C_{s12} to the sensor C_{12} (the detecting electrode). Hence, the charge is redistributed to develop voltage V_0, which can be measured.

Therefore, according to the charge conservation law:

$$\text{Total Charge } (Q) = C_{s12}V = C_{s12}V_0 + C_{12}V_0 \qquad \text{(B1)}$$

the unknown capacitance C_{12} can be obtained, as shown in Eq. B2:

$$C_{12} = Q/V_0 - C_{s12} \qquad \text{(B2)}$$

However, in such a switched capacitor configuration, the effects of electrostatics at capacitor C_{12} were not considered. In the present study, it was found that perturbations in the capacitance signal were due to charge accumulation. In pneumatic conveying of solids through a dielectric pipe, electrostatic charges are generated through particle-wall collisions. Charged particles not only affect the flow behavior but also affect the ECT measurements,[25] so an additional electrostatic term has to be considered on the LHS of Eq. B1:

$$Q + C_{12}V_s = C_{s12}V_0' + C_{12}V_0' \qquad \text{(B3)}$$

where V_s is the potential difference between the electrodes 1 and 2, taking into account electrostatic charges accumulated on the pipe wall; and V_0' is the measured voltage value.

Therefore, V_0' replaces V_0 in Eq. B2 and the unknown capacitance C_{12}' is calculated:

$$C_{12}' = (Q - C_{s12}V_0')/(V_0' - V_s) \qquad \text{(B4)}$$

Ideally, electrostatic charges are distributed uniformly; thus, $Vs = V_1 - V_2 = 0$, that is, the term arising due to electrostatics

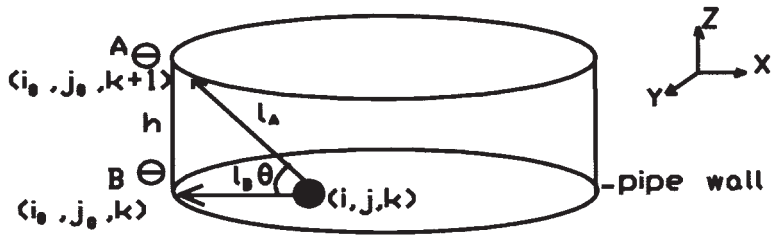

Figure A2. Enlarged sections AB from Figure A1 illustrating the contribution of electric field strength from neighboring axial actions.

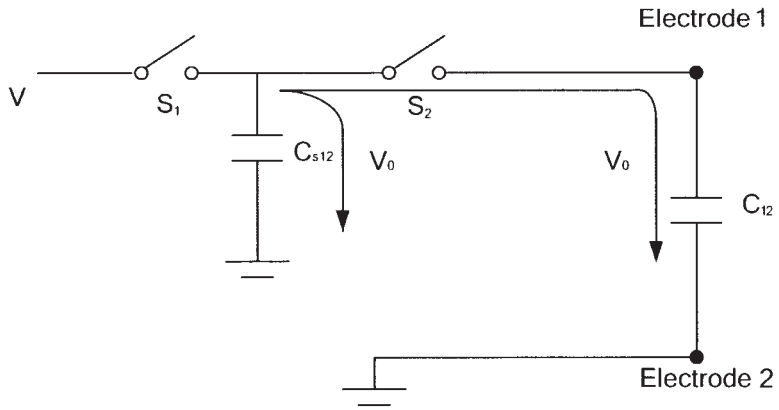

Figure B1. Switch capacitor configuration.

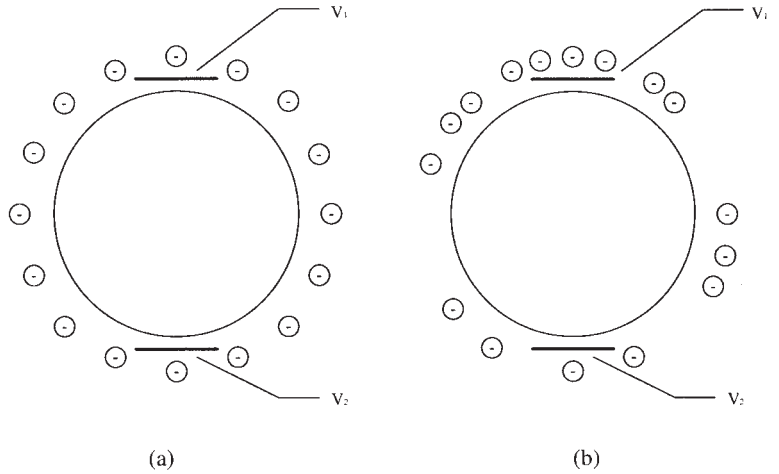

Figure B2. Spatial electrostatic charge distributions over a cross-section of conveying pipe:
(a) Uniform charge distribution; (b) non-uniform charge distribution.

can be eliminated, as shown in Figure B1. Therefore, $V_0' = V_0$ and $C_{12}' = C_{12}$; the measured values are the reflection of the true values.

However, in most cases, the static charge generation is not uniformly distributed, such as that due to gravity or pipe-curvature, one side of the pipe has much more particle impacts compared to the other side. For non-uniform charge distribution, $Vs = V_1 - V_2 \neq 0$, as shown in Figure B2, so that the electrostatics term cannot be neglected. Thus, $V_0' \neq V_0$ and correspondingly, $C_{12}' \neq C_{12}$; C_{12}' is a pseudo value of the unknown capacitance, which cannot be corrected unless the electrostatics term can be measured independently. This quantity of surface charge distribution is difficult to be measured using the current experimental setup. An analytical method will need to be developed to compensate the measurement error caused by non-uniform electrostatic charge distribution in the conveying pipe.

Manuscript received Feb. 25, 2006, and revision received July 15, 2006.